Article

Magnetophoretic Cell Sorting: Comparison of Different 3D-Printed Millifluidic Devices

Niclas Reiter [1], Jan Auchter [1], Marius Weber [1], Sonja Berensmeier [1] and **Sebastian P. Schwaminger [1,2,***

[1] Bioseparation Engineering Group, School of Engineering and Design, Technical University of Munich, Boltzmannstr. 15, 85748 Garching, Germany

[2] Otto-Loewi Research Center, Division of Medicinal Chemistry, Medical University of Graz, Neue Stiftingtalstr. 6, 8010 Graz, Austria

* Correspondence: sebastian.schwaminger@medunigraz.at; Tel.: +43-31638572125

Abstract: Cell sorting is a highly applicable technology for multiple biological, biotechnological, and medical applications. Magnetic cell sorting can be realized with microfluidic and millifluidic flow cells. Additive manufacturing and 3D printing allow for fast prototyping and validating separation processes on this small scale. Therefore, our novel approach is to use this technology to print millifluidic channels and to directly evaluate them on their magnetic separation performance and their handling for cell manipulation. In this study, two different flow cells manufactured with a 3D printer are compared in regard to their use for the magnetic cell sorting of algae. One linear flow cell geometry and one spiraling flow cell geometry have been investigated with perpendicular magnetic fields. Iron oxide nanoparticles have been synthesized and characterized prior to their use as a magnetic label for algae cells. Particle uptake by algae are investigated by a phenanthroline assay, and the particle/algae mixtures are studied by microscopy, dynamic light scattering, zeta potential, and magnetophoretic mobility measurements. Depending on magnetic susceptibility, the cells undergo different magnetophoretic forces. Interestingly, the spiraling geometry leads to a better fractionation of algae cells in accordance with their iron oxide load.

Keywords: millifluidic separation; microfluidic separation; nanoparticles; magnetic separation; cell sorting; fractionation; algae; iron oxide nanoparticles

1. Introduction

Cell sorting is an important analytical method to determine the size of different cells in biological samples [1]. This includes procaryotic cells as well as eucaryotic cells. Cell sorting allows for the classification and study of distinct cells. Especially fluorescence-activated cell sorting (FACS) and magnetic-activated cell sorting (MACS) are used for cell classification [1]. Both methods depend on the physical properties of cells, such as size and shape but also surface epitopes and surface charge of different cells. One possibility is to use distinct surface proteins to distinguish the different cell types by immunospecifically attaching either fluorophores (FACS) or magnetic nanoparticles (MACS) to the cell [2]. The method of MACS was introduced by Miltenyi et al., who used nanoscale superparamagnetic labels for the targeting of cells and magnetic microcolumns for the separation of multiple cells [3–5]. The magnetic separation is also the basis of the magnetic fractionation. Moore et al. [6] were among the first to build a magnetic flow sorter to fractionate T-lymphocytes, targeted with immunomagnetic colloid, according to cell surface marker expression. A similar setup was used by Schneider et al. [7] to sort stem and progenitor cells, which were immunomagnetically labeled with magnetic nanobeads. Both devices comprised a millimeter scale channel with multiple in- and outlets and a permanent magnet that, together with pole pieces, induced a nearly constant gradient of the magnetic force field perpendicular to the flow direction. Since the fractionation principle of both devices is dependent on a laminar flow pattern inside the channel, both the outlets and the inlets were

connected to syringe pumps precisely controlling the flow rates. Thus, a so-called transport lamina is created, a fraction of flow in the channel to which a cell must be driven in order to exit a particular outlet [7]. These devices sort cells according to their magnetophoretic mobility, which is a characteristic of a magnetic particle influenced by its susceptibility, the particle size, and the viscosity of the fluent medium [8]. However, there are multiple challenges with the cell sorting, which arise from the inhomogeneous magnetic fields and complex geometries of the cell sorters [9].

A typical representative of the third group is microfluidic magnetic separation, which, just like the macroscopic counterparts, uses an external magnetic field generated by a permanent or electromagnet to drive the separation of the target entity [4]. If this target entity is nonmagnetic (i.e., typical biological compound), functionalized magnetic nanoparticles bound to or internalized into the target are used to indirectly apply magnetic forces on the particles [4,10]. Depending on the magnitude of the magnetic field gradient employed, two types can be distinguished, the high-gradient magnetic separation (HGMS) and the low-gradient magnetic separation (LGMS). Like MACS, HGMS uses magnetizable structures, such as wires or particles, to create a high gradient of the magnetic field and, thus, a high magnetic force within the close range of the magnetizable substrate [4]. HGMS was used by Xia et al. [11] to successfully separate *E. coli* bound to magnetic particles from solutions containing red blood cells in a similar quantity as blood. They used a microstructured NiFe layer in the form of a microcomb to create a high gradient, which, in the presence of a simple permanent magnet, pulled the bacteria across the laminar streamline into a collection path. Chen et al. [9] also applied the concept of HGMS to concentrate and purify HIV viral products attached to magnetic particles from human plasma. Instead of a microcomb, they introduced iron particles into a microfluidic chamber to create a high gradient and trap the virions within the channel. The magnetic field was generated by a permanent magnet. Another active research field in which HGMS is applied is the detection of malaria-infected red blood cells. The stronger magnetic susceptibility induced by the conversion of hemoglobin into hemozoin in infected cells was used by Nam et al. [12] to separate malaria–infected cells from healthy ones. In contrast to HGMS, LGMS only uses a permanent magnet generating a nonuniform magnetic field to separate particles. The omission of the magnetizable substrate significantly reduces the magnetic force but, therefore, simplifies the setup. Lee et al. [13] came up with a setup using LGMS to also separate *E. coli* from whole blood samples. Unlike the device developed by Xia et al. [11], their microdevice exhibited only one inlet, and separation was effected by the accumulation of the bacteria at the channel walls adjacent to the magnets and not by the removal through one of the two outlets. Moreover LGMS was already used by Zeng et al. [14] to separate yeast cells from polystyrene microparticles in a microfluidic channel. The devices presented so far aim at the magnetic removal of a targeted entity out of a liquid, most of the time a nonmagnetic medium. An application that even goes a step further is the magnetic sorting of particles by their size or magnetic susceptibility. Here, Wu et al. [15] presented a microfluidic device to size-selectively separate magnetic nanospheres using a permanent magnet by deflecting the polydispersed particles from one inlet channel into two outlets. They demonstrated that larger, meaning more magnetic, particles were deflected stronger, resulting in a mean diameter difference of the nanospheres at the two outlets. This was also confirmed by the work of Solsona et al. [16], who used a 3D-printed microfluidic chip to sort single-catalyst particles according to their magnetic moment. The LGMS principle was also used by Pamme and Wilhelm [17,18], who sorted HeLa cells and mouse macrophages depending on their different magnetic susceptibility, which was achieved by different incubation times with magnetic nanoparticles.

Recently, the interaction of magnetic nanoparticles and different types of algae has been widely investigated. A lot of research focuses on the magnetophoretic separation of microalgae [19–22], since this has shown to be an efficient technique to harvest small algae and thus exploit their high potential as bioresource for nutrition or as biofuel feedstock. Magnetophoretic separation of algae was introduced in the 1970s [21,23] and, initially, was

presented as an effective water treatment, in order to remove algae blooms from water and avoid eutrophication. Despite this extensive research, it is not yet fully understood how the magnetic nanoparticles (MNPs) bind to the algae. Even though potential influencing factors, such as pH, salt concentration, particle size, and different coatings, have been investigated [19–21,24], it still has not been clarified which forces are primarily responsible for the adhesion process. In many publications, the electrostatic force is considered to be the leading effect for the adhesion and adsorption [25]. Studies on algae separation using MNPs with positively charged coatings [20,21] support this theory, since they demonstrate better harvesting efficiency for the coated MNPs compared with naked ones and attribute this effect to the enhanced electrostatic attraction to the inherent negatively charged algae surface. Nevertheless, separation experiments including uncoated MNPs show contradicting results. As an example, Fraga-Garcia et al. [19] studied the harvesting efficiency of microalgae using naked MNPs and observed only small effects due to pH and salt variation on the harvesting result. As a consequence, further explanation attempts, including nanosize effects, hydrophobic interactions, and the existence of locally distributed positive charges, were made [19,26,27]. To sum up, the adhesion process is certainly influenced by an interaction of the different forces and cannot be attributed to a single effect. In particular, the algae are living organisms that might change their behavior over time and are strongly influenced by environmental conditions.

In this study, we compare two different magnetic sorter geometries and their ability to magnetophoretically fractionate algae cells depending on the amount of attached nanoparticles. We want to emphasize the novelty of this study, comparing two millifluidic systems, which have been designed and 3D-printed, for the use of magnetic cell sorting and separation.

2. Results

The synthesized nanoparticles show a TEM diameter of around 9–10 nm and deviate in their size from 4 to 15 nm, as shown in Figure 1. The nanoparticles do not show a very homogeneous size or shape and also demonstrate aggregates on the TEM grits onto which they have been precipitated. The obtained results concerning the heterogeneity and particle size distribution are in good agreement with other previous works from our group [28,29].
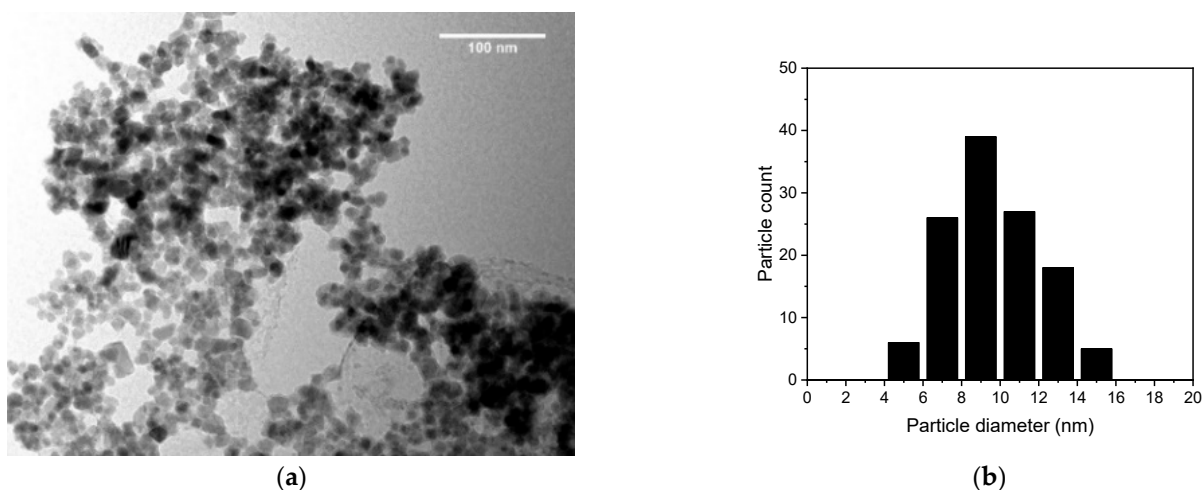

(**a**)

(**b**)

Figure 1. (**a**) Transmission electron microscopy (TEM) microphotography of bare iron oxide nanoparticles (MNPs) and (**b**) the size distribution of the particles on the right.

The nanoparticles can be identified as nanoscale iron oxide nanoparticles that mainly contain magnetite according to the XRD data shown in Figure 2a [30]. Here, the distinct reflections of the 311 plane as well as the 440, 220, 511, and 400 planes strongly indicate magnetite especially since no reflections corresponding to maghemite can be identified. However, due to the nanoscale of the particles indicated by the peak broadening,

maghemite cannot be excluded as a phase [30]. The synthesized nanoparticles are super-paramagnetic and show a low remanence (<1 Am^2/kg) and a high saturation magnetization of around 82 Am^2/kg at 300 K [31]. Furthermore, the nanoparticles have a high relative permeability of up to 9 in low magnetic fields (below 200,000 A/m), which is our most important property to influence these particles in a magnetic field and is visualized in Figure 2. The permeability decreases in higher fields since the saturation is reached [28,32].
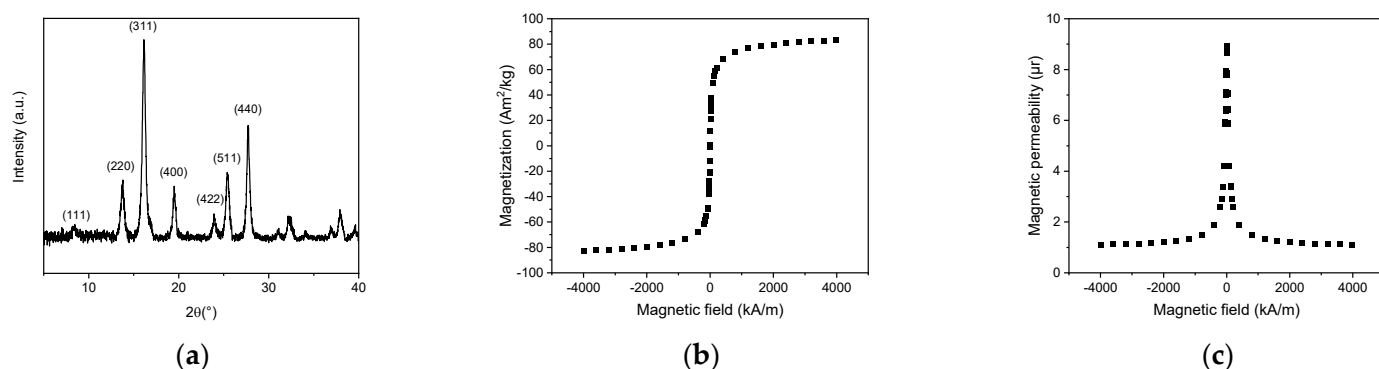

(a)　　　　　　　　　　　　**(b)**　　　　　　　　　　　　**(c)**

Figure 2. (**a**) X-ray diffractogram of the synthesized iron oxide nanoparticles obtained with a Mo Kα source in transmission [33]. Magnetization curves (**b**) and relative magnetic permeability (**c**) obtained with SQUID of the synthesized iron oxide nanoparticles at 300 K.

The magnetic particles demonstrate an amphoteric behavior and show a positive zeta potential at low pH values and negative zeta potential at high pH values. This behavior is in good agreement with previous studies of similar particles under similar conditions [29]. The sucrose solution, which allows an easy handling in the millifluidic device, slightly shifts the isoelectric point from around pH 7 to pH 6 [28]. This can be observed as overall charge as well as particle size distribution of the hydrodynamic diameter (Figure 3). Here, the particles dispersed in sucrose solution show a lower hydrodynamic diameter than the particles in deionized water at pH > 7. The particle diameters vary from around 100 nm at low pH values in water to a maximum of more than 3 μm at ambient pH conditions. At higher pH values, the hydrodynamic diameter decreases again to around 1000 nm. At low pH values, the particle aggregates are visible, which form nonstable agglomerates at zeta potentials closer to zero. The high colloidal stability of the nanoparticles in sucrose at pH 7–11 is another great advantage in addition to the higher viscosity compared with deionized water. The particles in sucrose dispersion are colloidally stable with aggregates demonstrating less than 300 nm hydrodynamic diameters at all pH values higher or equal to 7. On the other hand, the particles dispersed in water are not stable at neutral pH conditions between pH 6 and pH 11. Here, the maximum hydrodynamic diameters reach 6 μm at pH 5 and 6, while the hydrodynamic diameter decreases with higher pH values in sucrose to diameters of around 150 nm. This discrepancy of the hydrodynamic diameter of the formed particle aggregates at similar electrochemical stabilization, since the zeta potential is very similar, indicates a thermodynamic diffusion effect, which is dependent on the viscosity of the surrounding fluid [29].
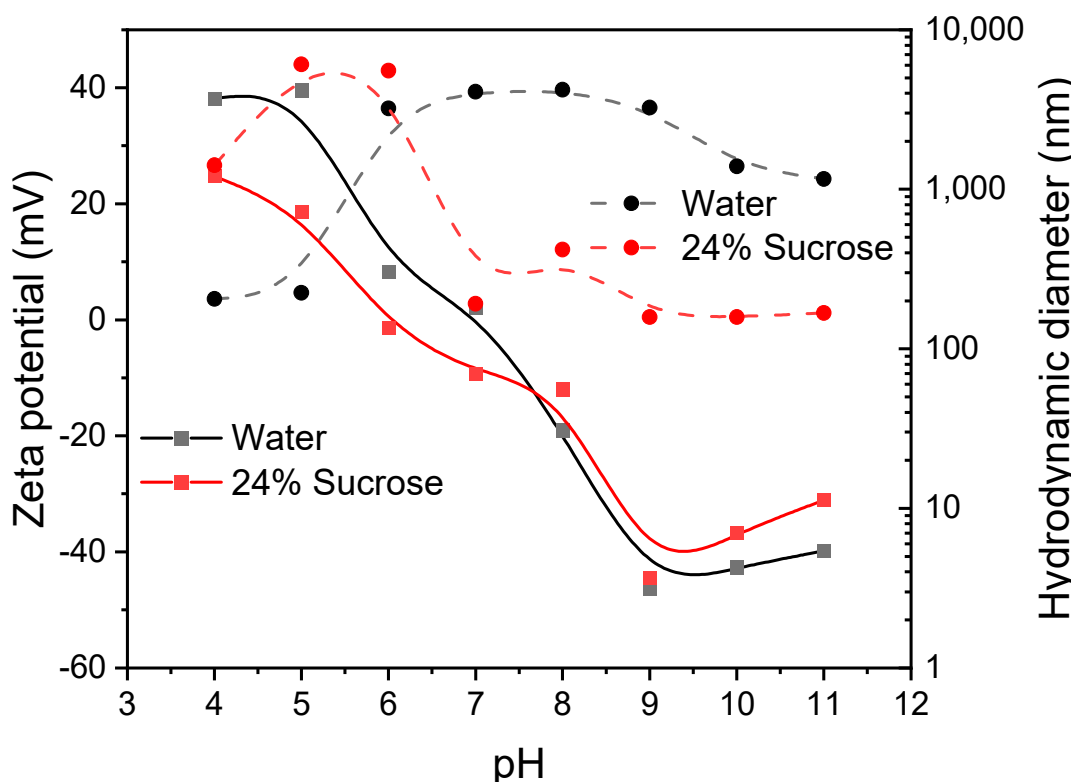
Figure 3. Zeta potential and DLS of iron oxide nanoparticles (2 g/L) over the pH range 4–11 at 25 °C in deionized water and sucrose containing water (24.4 w%).

Not only the properties of the magnetic nanoparticles are crucial for the separation of algae cells, but also the algae play an important role in the particle binding to the cells and to the agglomeration of both components. The zeta potential has been investigated for pure algae cells as well as for different mixtures of magnetic nanoparticles to algae cells (5:1, 1:1, and 1:5). Figure 4a highlights the zeta potential dependence on different amounts of nanoparticles and algae. Algae cells demonstrate a negative zeta potential in the whole pH range between 4 and 11 between −30 and −40 mV. The mixture containing the fivefold algae concentration in comparison with the nanoparticles demonstrates a very similar behavior and slope as the pure algae cells. At an equal concentration of algae and nanoparticles, the zeta potential is still negative over the whole pH range. However, a distinct increase in the zeta potential can be observed at acidic pH values. When the fivefold particle concentration is monitored, the zeta potential even reaches positive values at low pH, even though the zeta potential is still influenced by the larger algae cells as well. To better understand the millifluidic simulation, we also conducted magnetophoretic sedimentation experiments (Figure 4b–d). The cumulative velocity distribution demonstrates very slow velocities of pure algae cells, which only sediment at speeds between 0.1 and 10 μm/s, while the magnetic content significantly affects the sedimentation velocity in a magnetic field. Here, the mixtures at low pH show a significantly higher sedimentation velocity than particles at higher pH. This trend is similar for all mixtures but less significant for mixtures containing lower magnetic particle concentrations. Moreover, a higher content of magnetic nanoparticles leads to higher median sedimentation velocities, which can be attributed to a greater magnetic particle content bound to algae cells as well as to a greater magnetic convection [4,31,34].
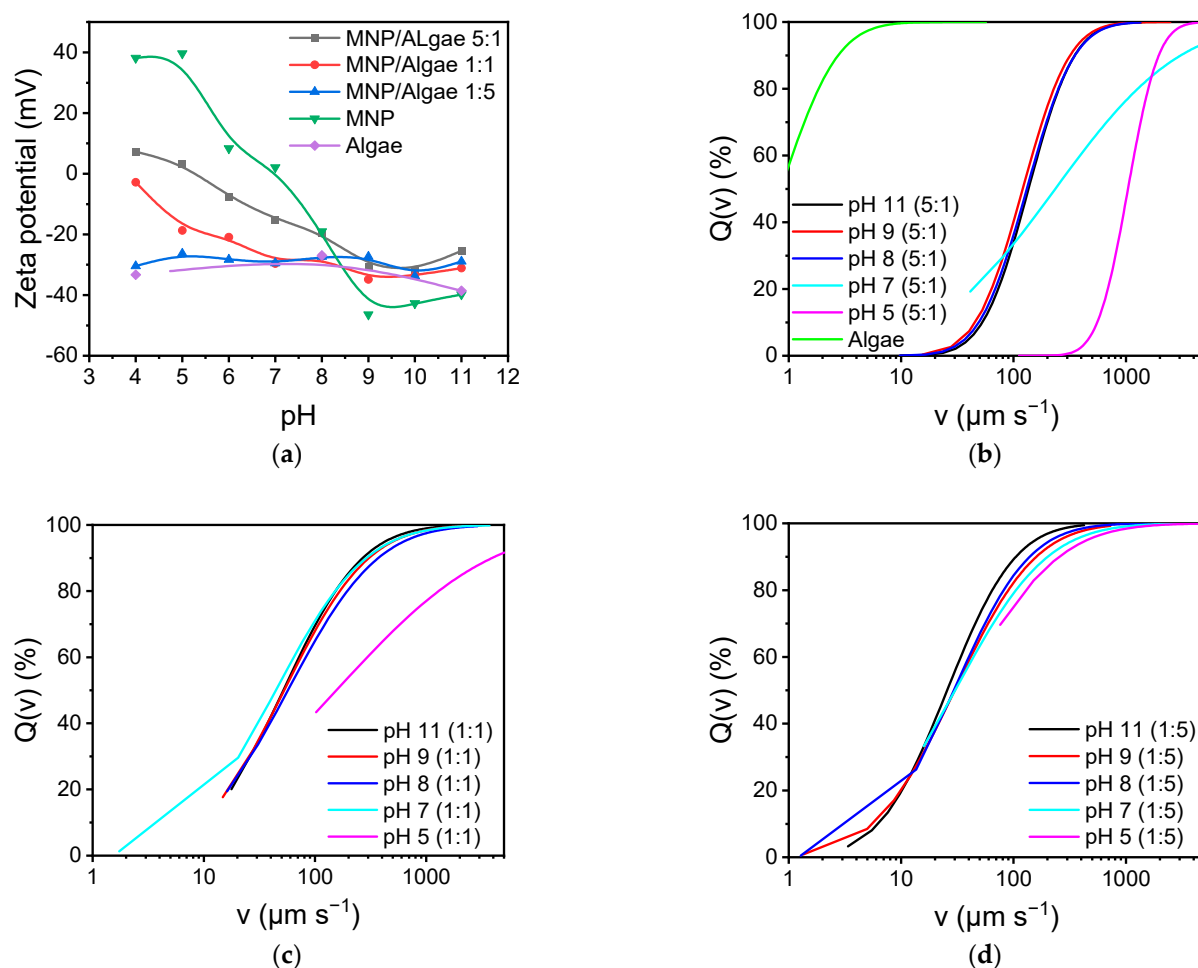
Figure 4. (**a**) Zeta potential of iron oxide nanoparticles (2 g/L) mixed with algae over the pH range 4–11 at 25 °C in sucrose containing water (24.4 w%). Cumulative distribution of sedimentation velocity of MNP and algae mixtures. (**b**) 5:1, (**c**) 1:1, and (**d**) 1:5.

With the particle properties being physically described, we further investigated the behavior of the nanoparticles in a simple millifluidic systems. Here, the influence of the pH and the respective zeta potential as well as the hydrodynamic diameter on the separation properties is evaluated.

In the following Figure 5, the working principle of the millifluidic cell is shown at a 70 µL/min flowrate in a sucrose solution (24.4 w%) at different pH values ranging from 7 to 11. While the flow of the magnetic nanoparticles (2 g/L) is not affected without a magnetic field, the influence of a magnetic field on the nanoparticles can be shown. Thus, this is a proof of concept that the separation and a fractionation in this millifluidic cell are possible. The higher pH values (10 and 11) showed the best separation properties. The flow in all cells is laminar, and the mixing effect is therefore solely driven by the diffusion of magnetic nanoparticles. The separation in the magnetic field, however, not only is due to magnetophoretic contributions but also includes effects of magnet-induced aggregation and magnetic convection [4,31]. The magnetic convection is thereby mostly dependent on the magnetic field gradient and the particle concentration, while the magnet-induced aggregation is also dependent on the electrostatic stabilization of magnetic nanoparticles. Hence, the magnetic separation is different at different pH values, as shown in Figure 5. While the particles possessing a zeta potential closer to zero at pH 7 show a significantly stronger magnetic separation effect, the particles at pH 9–11 show a broader distribution of particle separation in the millifluidic chips. Fewer particles are fully separated but also exit at outlets b and c.
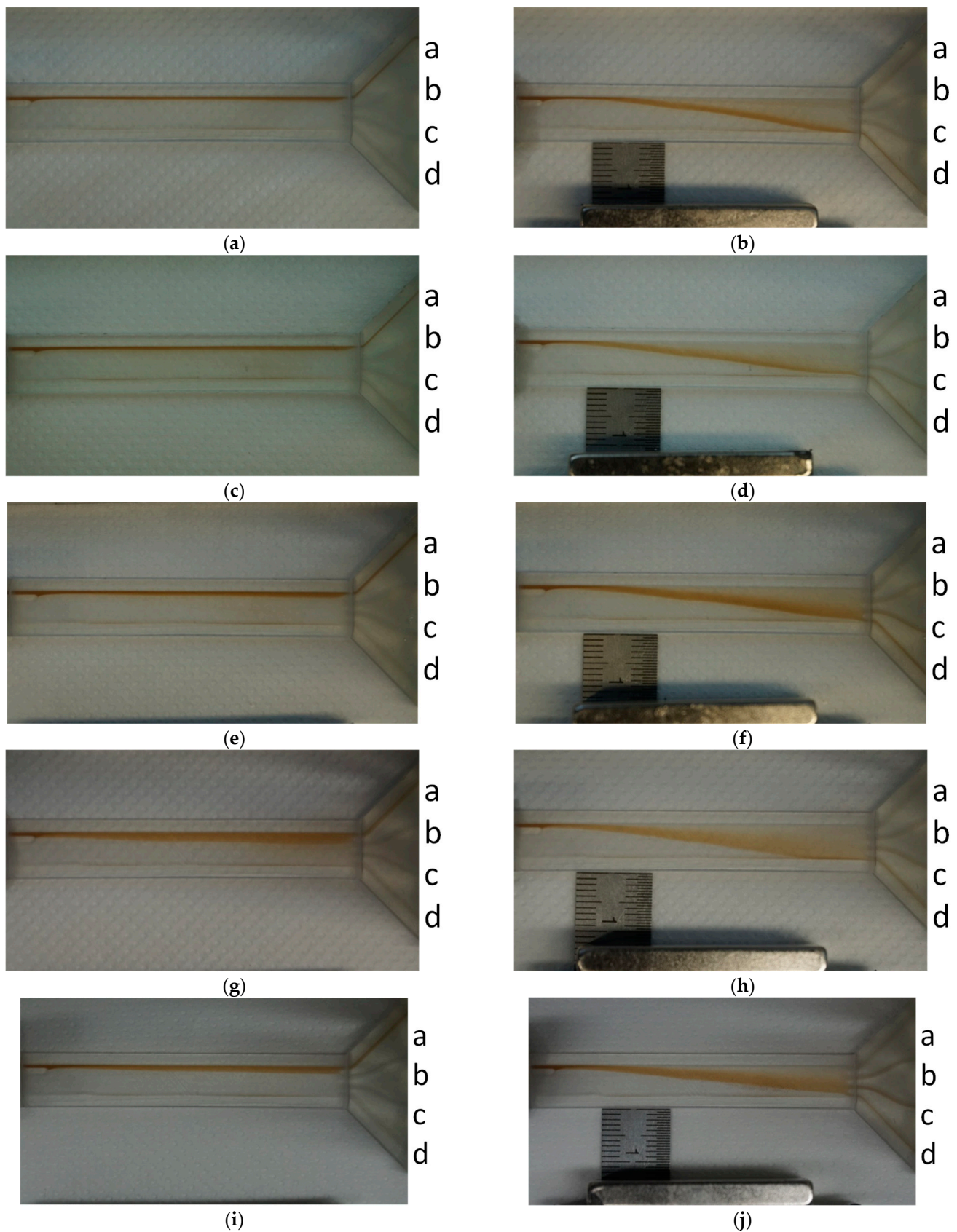
Figure 5. Separation of bare MNPs at pH 7 without (**a**) and with (**b**) magnet. Separation of bare MNPs at pH 8 without (**c**) and with (**d**) magnet. Separation of bare MNPs at pH 9 without (**e**) and with (**f**) magnet. Separation of bare MNPs at pH 10 without (**g**) and with (**h**) magnet. Separation of bare MNPs at pH 11 without (**i**) and with (**j**) magnet.

While the flow of the magnetic nanoparticles (2 g/L) is not affected without a magnetic field, the influence of a magnetic field on the nanoparticles can be shown. Thus, this is a proof of concept that the separation and a fractionation in this millifluidic cell is possible. The higher pH values (10 and 11) showed the best separation properties.

The same effects have been tested in the spiral system at pH 9 (Figure 6). Here, the effects are very similar in comparison with the straight millifluidic channel. Without an applied magnetic field, the magnetic particles are not drawn to any other exit but exit in exit a. However, if a field is applied, almost no particle exits in exit a, but the particles are distributed and cumulate especially in exits b and c. This indicates a distinct influence of the magnet on the particle distribution within the millifluidic system. Hence, this is proof that magnetic manipulation can also be conducted in this millifluidic geometry with bare iron oxide nanoparticles at pH 9. The separation splitting is much more pronounced in this geometry since the magnetic field is passed three times (with an increasing gradient). Therefore, this geometry seems more promising to have a better separation distribution of cells bound to fewer and to more magnetic particles. However, the spiraling geometry is also more complex and more challenging to process than the straight millifluidic cell.
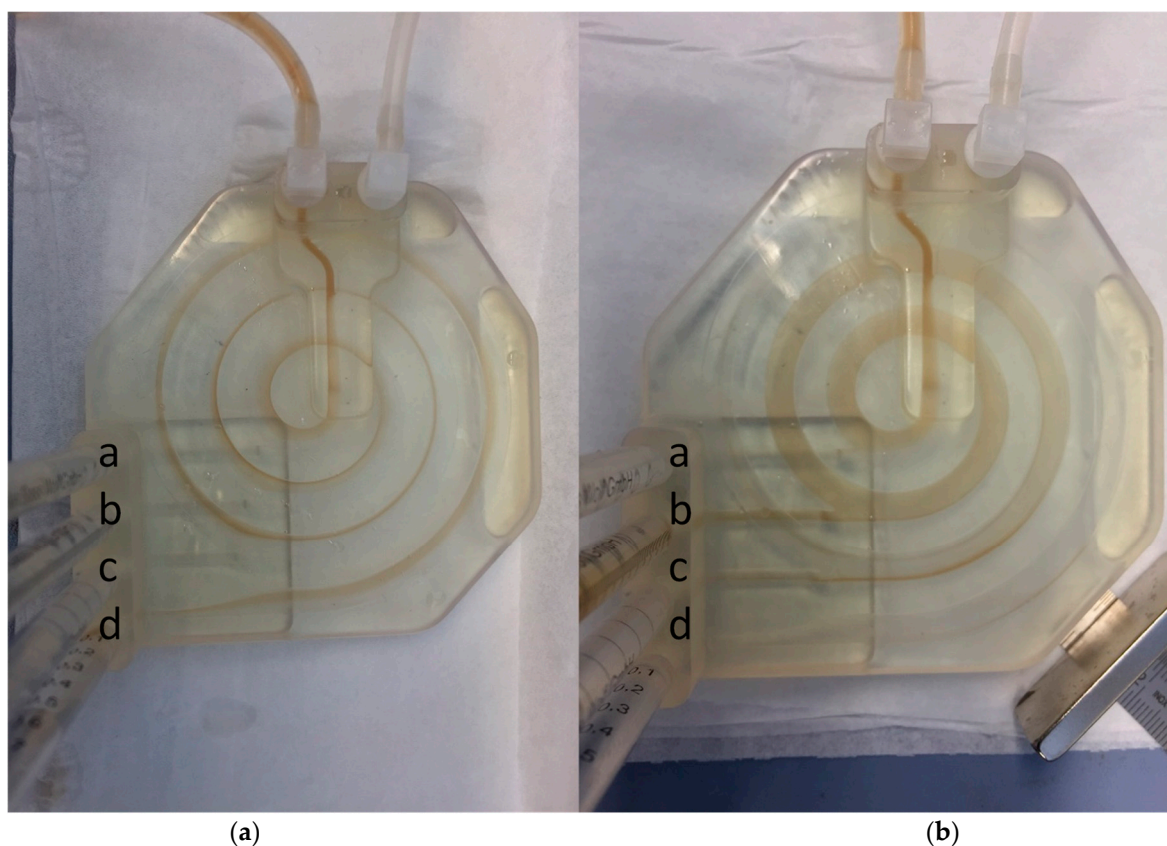

(**a**)　　　　　　　　　　　　　　　　　　　　　　　　(**b**)

Figure 6. Separation of bare MNPs at pH 9 without (**a**) and with (**b**) magnet.

With the proof of concept of the magnetic separation of magnetic nanoparticles in the millifluidic cells, the next step is the separation of living cells. Here, algae cells have been chosen since they can be detected easily with UV–VIS spectroscopy. For the first chip, the straight millifluidic cell, the outlets have been named a–d, which are closest to the inlet, and d, which is closest to the magnet. In an experiment where algae and magnetic particles and pure algae cells have been mixed and are flown through the chip, we can monitor distinct differences between both species (Figure 7a). While the pure algae cells mainly follow the laminar flow and exit at outlet a, most of the algae mixed with particles exit at outlet d. Therefore, the algae mixed with magnetic nanoparticles have been magnetically separated in this cell. The difference of magnetic nanoparticles with or without an applied magnetic

field is even more pronounced (Figure 7b). While magnetic particles are not separated when no magnetic field is applied, the application of a magnetic field leads to a separation, and therefore, the particles mainly exit in outlet d.
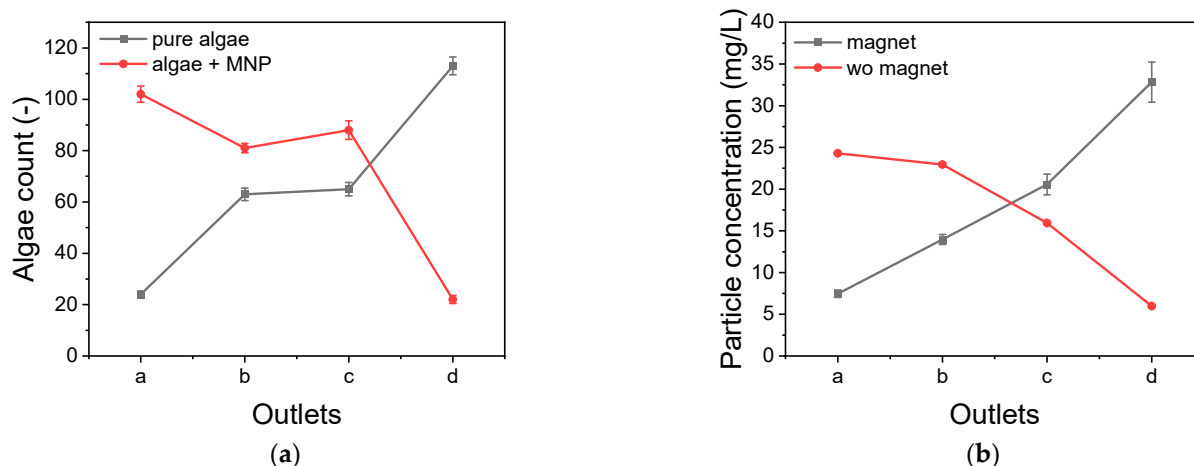

Figure 7. Separation process in millifluidic chamber 1. (**a**) Algae count from the Neubauer counting chamber for algae and mixtures of algae and magnetic nanoparticles. (**b**) Magnetic particle concentration determined with phenanthroline assay for separation with and without (wo) magnet.

In the second geometry, not only magnetic forces but also spiraling forces, such as the Dean force, play a role for the separation of cells. In a comparison of pure algae cells and algae cells mixed with magnetic nanoparticles, a distinct distribution can be monitored in a magnetic separation setup. While the pure algae cells are not separated and mainly exit at outlet a (which is closest to the magnet), most of the algae in the mixed suspension exit through outlet d. Here, the magnetic separation leads to a magnetophoretic manipulation of the cells, and therefore, the algae already exit mostly through the first outlet (Figure 8a). Interestingly, the distribution of magnetic particles without and with an applied magnetic field is much closer together in this geometry. Here, most of the particles with and without an applied magnetic field exit the first outlet (d). However, the trend is much more significant for the applied field compared with the no applied field (Figure 8b). This means that this geometry is more suitable for an effective cell separation according to the magnetic content, while it is more challenging to separate magnetic particles depending on their magnetic properties.
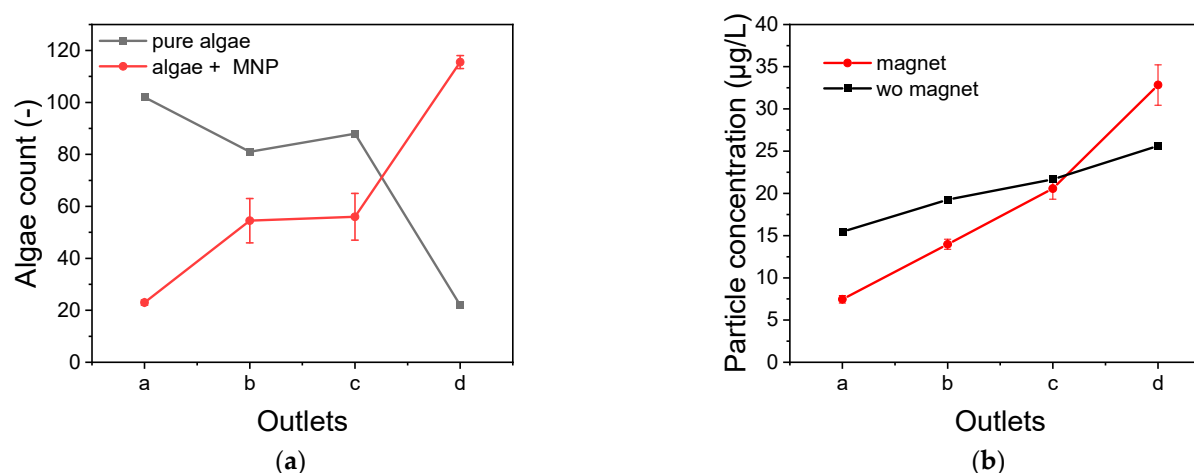

Figure 8. Separation process in millifluidic chamber 2. (**a**) Algae count from the Neubauer counting chamber for algae and mixtures of algae and magnetic nanoparticles. (**b**) Magnetic particle concentration determined with phenanthroline assay for separation with and without (wo) magnet.

3. Discussion

The results clearly indicate the we synthesized iron oxide nanoparticles, which are mainly composed of magnetite, even though maghemite cannot be completely excluded [28,35]. The particles demonstrate single particle sizes of around 10–12 nm and are in great agreement with previous studies [35]. However, no single particles have been observed with dynamic light scattering, but the smallest aggregates observed range at around 100–200 nm. The agglomeration of these nanoparticles is dependent on the environment, and therefore, the hydrodynamic diameter of agglomerates increases with zeta potentials, which are closer to zero [31,36,37]. This behavior can be observed, as well as the effect of sucrose content. The sucrose content only slightly affects the zeta potential but significantly affects the agglomeration behavior. This effect can be related to the surface effect of sucrose but is mainly due to the viscosity difference of water and sucrose containing water. Aside from the sucrose content, the pH plays an important role for nanoparticle stabilization and nanoparticle agglomeration [29]. At pH values close to 7, the zeta potential of the iron oxide nanoparticles is close to zero, and therefore, the particles tend to agglomerate, while the nanoparticles are mostly stable at higher and lower pH values. This behavior is in very good agreement with the literature [29]. The pH affects not only the agglomeration but also the binding behavior to algae cells. The higher viscosity of sucrose-containing solutions also affects the sedimentation, and therefore, magnetic particles and magnetic particle algae mixtures sediment with lower velocity than in sugar-free water. The pH and the agglomeration can also be observed in the magnetic sedimentation experiments. A more pronounced particle agglomeration leads to higher sedimentation velocities [31]. In addition to the agglomeration behavior, the total content of magnetic nanoparticles affects the magnetophoretic sedimentation behavior. A higher content of nanoparticles leads to higher median sedimentation velocities. While the sedimentation analysis allows for a great distinction of different velocities, the effect of magnetic fields on magnetic particles has also been studied in two different millifluidic systems. Here, the magnetic separation effect is very well visible and similarly dependent on the pH as already observed in the sedimentation experiments. Both millifluidic systems allow for a great magnetic separation of algae cells. However, the straight system allows for a better separation or fractionation of magnetic particles, while the spiraling system allows for a better separation of algae cells bound to magnetic particles. We want to emphasize the significant differences for the magnetic separation at different pHs, which significantly affect the aggregation behavior of iron oxide nanoparticles and, therefore, the magnet-induced aggregation [31]. Hence, this also affects the separation process and the diffusion of iron oxide nanoparticles. On the other hand, we were able to show that a magnetic manipulation of algae cells is possible in different millifluidic geometries, once the aggregation challenge is overcome. Fifty percent of all algae cells are maximally magnetically separated in the first geometry when introduced to iron oxide nanoparticles, while almost no cells exit the outlet closest to the magnet without magnetic cells. There are still multiple issues to overcome to really be able to control a magnetic separation process in a millifluidic setup with these particles, and there needs to be more investigation on the aggregation behavior.

The novelty of this study is the comparison of two different millifluidic separation systems that have been 3D-printed. The behavior of magnetic nanoparticles in these different systems and in flow and magnetic fields is addressed, and with this study we want to emphasize the challenges of magnetic separation processes due to the nature of magnetic nanoparticles and their magnet-induced aggregation as well as their convective behavior in magnetic fields.

4. Materials and Methods

4.1. Synthesis

In accordance with Roth et al., 35.0 g of iron (II) chloride and 86.4 g of iron (III) chloride, obtained from Sigma-Aldrich, were dissolved and mixed in 200 mL of deionized water. Sodium hydroxide (1 M), obtained from Fluka, was prepared with deionized water and

filled in a stirred tank glass reactor under a nitrogen atmosphere and under a stirring rate of 500 rpm with a blade stirrer [33]. Subsequently, the salt solution was added dropwise, which immediately formed a black precipitate. After complete addition, the reaction was continued for half an hour under constant conditions at 30 °C. The resulting particles were washed several times with deionized water until a conductivity of less than 200 S/cm was reached. All chemicals were used from the providers without further purification (reagent grade).

4.2. Characterization of MNP

Transmission electron microscopy (TEM) was carried out with a JEM 1400 Plus microscope from JEOL, and the recorded images were subsequently evaluated using the ImageJ software. Diluted nanoparticle suspensions were precipitated on carbon copper grids prior to TEM measurements. Around 100 particles per nanoparticle type were measured. X-ray diffraction (XRD) was recorded with a STOE Stadi P diffractometer with a molybdenum radiation source from STOE and Cie. The freeze-dried samples were mounted in transmission geometry and measured while rotating at room temperature for 30 min in the 2θ range of 2° to 50°. The magnetic susceptibility of the nanoparticles is determined by a SQUID characterization. For this work, a Quantum Design MPMS 5XL SQUID magnetometer was used. The measurements were carried out at 300 K in magnetic fields varying between −4 and 4 MA/m. Zetapotential and hydrodynamic diameters were determined over a pH range of 4 to 11 with a Beckman Coulter Delsa Nano. Dynamic light scattering was utilized to determine the hydrodynamic diameter of the particles and the algae particle compounds over a pH range of 4 to 11.

For the preparation of MNP dispersion, the MNPs were diluted to a concentration of 2 g/L using distilled water. The viscosity of the used MNP dispersions was increased by adding 24.4 wt% of sucrose, which increased the dynamic viscosity η by a factor of 2.5, compared with pure distilled water. The MNP–algae mixtures were prepared with the algae *Nannochloropsis salina*, which were cultivated and provided by the Institute of Biochemical Engineering of the Technical University of Munich. Mixtures of three different MNP/algae mass ratios were investigated. They were prepared by mixing an algae suspension with an initial mass concentration of 0.5 gL^{-1} with MNP suspension of appropriate concentration in order to obtain MNP/algae mass ratios of 1:5, 1:1, and 5:1. After mixing, 24.4 wt% of sucrose was added in order to increase the viscosity.

The MNP concentration was determined with a colorimetric assay using the organic molecule 1,10-o-phenanthrolin in accordance with the method described by Bäumler et al. [16,38].

Space and time resolved extinction profiles. A customized LUMiReader device was used to measure space- and time-resolved extinction profiles (STEP technology, LUM GmbH, Berlin, Germany) of the algae mixtures. After pH adjustment of the sample, an optical plastic cuvette was placed in a specially designed sample holder equipped with five disc magnets underneath the cuvette [39]. For the measurements, 2.5 µL of sample was pipetted into the cuvette, which was right afterwards placed into the measurement device at a constant temperature of 21 °C. The transmittance of parallel light featuring three different wavelengths (830, 630, and 410 nm) is detected across the entire vertical sample height (up to 40 mm) at adjustable time intervals. The obtained transmittance profiles are integrated over the sample height, leading to an integral transmittance for each time of measurement. The magnetic flux density and gradient of the field averaged through the probe height amounted to 66 mT and 0.14 T/m, respectively.

4.3. Millifluidic Experiments

Both fluidic chips were designed in Catia V5 and printed with a stereolithography printer (Formlabs, Berlin, Germany). To guarantee translucency, a clear resin was applied. In order to remove the resin from the outer surface, the printed parts were agitated in isopropyl alcohol for 20 s and immersed in the solvent for another 4 min. The procedure was repeated once. The inner, enclosed channels were flushed for 30 s with a syringe filled

with isopropyl alcohol. Subsequently, compressed air was driven through the channels to fully drain and dry the channels.

4.4. Chip 1

The fabricated millifluidic chip consists of two inlets, a broader one for the buffer solution and a narrower one for the particles or cells to be sorted. The inlets lead to a 35 mm long and 6.25 mm wide channel, where the sorting takes place. This main channel leads to four outlets. The thinner inlet channel and the outlets feature a width of 1 mm, which has shown to be the minimal width for fabrication, without irreversibly clogging the channels during 3D printing. The buffer inlet has a width of 5.25 mm. All channels have the same depth of 1 mm. The top of the device is 1 mm thick, the bottom 2 mm (Figure 9).
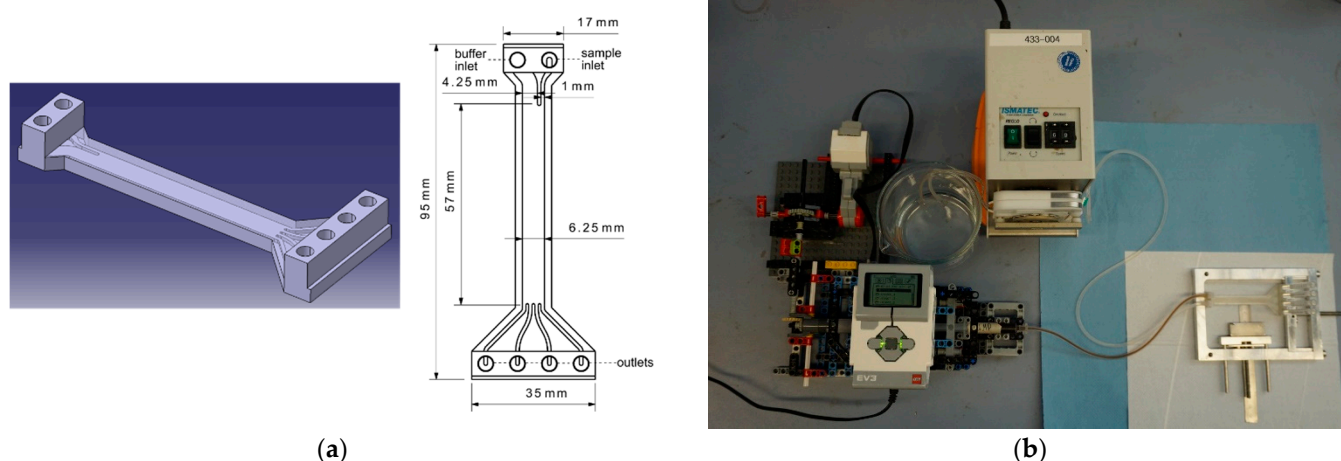

(**a**)   (**b**)

Figure 9. (**a**) Three-dimensional model and top view of the printed millifluidic chip. The sorting device features two inlets, one for the buffer and one for the samples to be sorted. During the passage, the particles are deflected into four different outlets. (**b**) Complete setup of the yeast sorting apparatus.

4.5. Chip 2

The chip has two inlets and four outlets, which can be contacted with Luer-lock fittings, and is designed in a spiraling shape. The chip has a basis size of 85.4 mm × 85 mm × 14 mm, even though the inlets have an additional height of 6 mm, leading to a 6 mm height at this position. The main channel has a cross section of 5 mm × 2 mm from two inlets (2.75 mm × 2 mm and 1.75 mm × 2 mm). The four outlets have a cross section of 2 mm × 2 mm each (Figure 10).
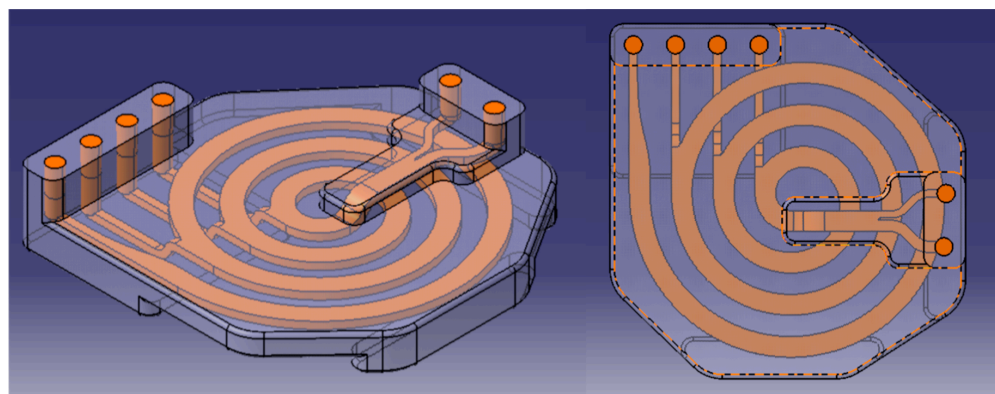

Figure 10. Three-dimensional model and top view of the printed millifluidic chip. The sorting device features two inlets, one for the buffer and one for the samples to be sorted. During the passage, the particles are deflected into four different outlets.

A syringe pump for standard 3 mL syringes was constructed using LEGO Mindstorms bricks. The setup shown in Figure 9 is similar to the ones described elsewhere [40]. Its function is based on a LEGO® stepper motor, which provides the necessary torque to push the syringe plunger. To do so, the rotary motion of the motor is transduced by an actuator into a linear movement of a LEGO® frame, which is guided by four rods and transmits the force to the plunger. For achieving the desired low flow rates, a reduction gear box is used to step down the speed of the motor. Therefore, a worm gear was combined with a 24-teeth gear wheel, resulting in a step-down ratio of 1:24. The speed of the motor and thus the flow rate is controlled by a LEGO® EV3 control brick that was programmed using the LEGO® Mindstorms software. The described assembly is capable of delivering flow rates between 70 and 1300 µL min^{-1}.

For providing a fluidic flow, the assembled pump and an ISMATEC ISM 795C tubing pump are used.

4.6. Particle Separation

The sample suspension was drawn up with the 3 mL syringe and pumped into the chip with the assembled pump. The position of the magnet was adjusted until the sample was deflected to all four outlets. After the right distance was found (6–7 mm), the reservoirs were emptied simultaneously using a multichannel pipette. For the evaluation of the sorting process, samples of each outlet were continuously taken with the multichannel pipette and filled into 2 mL Eppendorf tubes. The outlets were numbered from a to d, where a is the outlet farthest away from the magnet and d the one closest to the magnet. The obtained specimens were analyzed regarding algae and MNP concentration. The latter was ascertained with a phenanthroline assay. Algae concentration was determined by visual counting in a Neubauer improved counting chamber. Microscopic images were made with an AXIO Observer 7 from Zeiss with differential interference contrast and an Axiocam 506 mono. Phase contrast and fluorescent images were made and, subsequently, superimposed to better visualize algae cells. In order to excite the chlorophyll within the algae, an excitation light of 475 nm, provided by an integrated LED, was applied. The obtained images were postprocessed and superimposed. For the determination of the algae concentration, 10 inner squares of the chamber were counted out and the results averaged. The digital camera was again used to document the flow within the chip.

5. Conclusions

This study compares two different designs of millifluidic cells for the separation of cells with magnetic nanoparticles. The study demonstrates the use of different millifluidic cells and that both are able to separate algae cells attached to magnetic nanoparticles. The magnetic particle content determines the magnetophoretic separation behavior. The magnetic particles have been characterized thoroughly towards their size, aggregation, phase, and magnetic properties. In addition to the particle content, the agglomeration behavior of bare iron oxide nanoparticles and magnetic nanoparticle algae mixtures plays a significant role for the magnetic separation. To control the magnetic separation behavior, the pH and the viscosity of the solvent can be adapted. A higher sucrose content and, therefore, a significantly higher viscosity lead to smaller particle agglomerates at ambient pH and, therefore, to a better control of the magnetic separation behavior. The separation behavior is verified by magnetic sedimentation experiments and millifluidic separation experiments. An important finding is that sucrose is a very suitable environment for effective cell separation. Thus, this study helps to better understand the magnetic separation of cells, such as algae cells. We believe that these systems can also be suitable for the separation of other procaryotic and eucaryotic cells and that the aggregation behavior in these millifluidic cells distinctly contributes to the understanding of the magnetic separation of iron oxide nanoparticles. Therefore, this study can contribute to future magnetic separation applications.

References

1. Cocovi-Solberg, D.J.; Worsfold, P.J.; Miró, M. Opportunities for 3D printed millifluidic platforms incorporating on-line sample handling and separation. *Trends Anal. Chem.* **2018**, *108*, 13–22. [CrossRef]
2. Lee, W.; Tseng, P.; Di Carlo, D. Microfluidic Cell Sorting and Separation Technology. In *Microtechnology for Cell Manipulation and Sorting*; Lee, W., Tseng, P., Di Carlo, D., Eds.; Springer International Publishing: Cham, Switzerland, 2017; pp. 1–14. ISBN 978-3-319-44137-5.
3. Miltenyi, S.; Müller, W.; Weichel, W.; Radbruch, A. High gradient magnetic cell separation with MACS. *Cytometry* **1990**, *11*, 231–238. [CrossRef] [PubMed]
4. Leong, S.S.; Yeap, S.P.; Lim, J. Working principle and application of magnetic separation for biomedical diagnostic at high- and low-field gradients. *Interface Focus* **2016**, *6*, 20160048. [CrossRef] [PubMed]
5. Theel, E.K.; Schwaminger, S.P. Microfluidic Approaches for Affinity-Based Exosome Separation. *Int. J. Mol. Sci.* **2022**, *23*, 9004. [CrossRef]
6. Moore, L.R.; Zborowski, M.; Sun, L.; Chalmers, J.J. Lymphocyte fractionation using immunomagnetic colloid and a dipole magnet flow cell sorter. *J. Biochem. Biophys. Methods* **1998**, *37*, 11–33. [CrossRef]
7. Schneider, T.; Karl, S.; Moore, L.R.; Chalmers, J.J.; Williams, P.S.; Zborowski, M. Sequential CD34 cell fractionation by magnetophoresis in a magnetic dipole flow sorter. *Analyst* **2010**, *135*, 62–70. [CrossRef]
8. Zhou, C.; Boland, E.D.; Todd, P.W.; Hanley, T.R. Magnetic particle characterization-magnetophoretic mobility and particle size. *Cytometry* **2016**, *89*, 585–593. [CrossRef]
9. Chen, L.; Yang, C.; Xiao, Y.; Yan, X.; Hu, L.; Eggersdorfer, M.; Chen, D.; Weitz, D.A.; Ye, F. Millifluidics, microfluidics, and nanofluidics: Manipulating fluids at varying length scales. *Mater. Today Nano* **2021**, *16*, 100136. [CrossRef]
10. Gijs, M.A.M. Magnetic bead handling on-chip: New opportunities for analytical applications. *Microfluid. Nanofluid.* **2004**, *1*, 22–40. [CrossRef]
11. Xia, N.; Hunt, T.P.; Mayers, B.T.; Alsberg, E.; Whitesides, G.M.; Westervelt, R.M.; Ingber, D.E. Combined microfluidic-micromagnetic separation of living cells in continuous flow. *Biomed. Microdev.* **2006**, *8*, 299–308. [CrossRef]
12. Nam, J.; Huang, H.; Lim, H.; Lim, C.; Shin, S. Magnetic separation of malaria-infected red blood cells in various developmental stages. *Anal. Chem.* **2013**, *85*, 7316–7323. [CrossRef]
13. Lee, J.-J.; Jeong, K.J.; Hashimoto, M.; Kwon, A.H.; Rwei, A.; Shankarappa, S.A.; Tsui, J.H.; Kohane, D.S. Synthetic ligand-coated magnetic nanoparticles for microfluidic bacterial separation from blood. *Nano Lett.* **2014**, *14*, 1–5. [CrossRef] [PubMed]
14. Zeng, J.; Deng, Y.; Vedantam, P.; Tzeng, T.-R.; Xuan, X. Magnetic separation of particles and cells in ferrofluid flow through a straight microchannel using two offset magnets. *J. Magn. Magn. Mater.* **2013**, *346*, 118–123. [CrossRef]
15. Wu, J.; Yan, Q.; Xuan, S.; Gong, X. Size-selective separation of magnetic nanospheres in a microfluidic channel. *Microfluid. Nanofluid.* **2017**, *21*, 47. [CrossRef]
16. Solsona, M.; Nieuwelink, A.-E.; Meirer, F.; Abelmann, L.; Odijk, M.; Olthuis, W.; Weckhuysen, B.M.; van den Berg, A. Magnetophoretic Sorting of Single Catalyst Particles. *Angew. Chem. (Int. Ed. Engl.)* **2018**, *57*, 10589–10594. [CrossRef] [PubMed]
17. Pamme, N.; Wilhelm, C. Continuous sorting of magnetic cells via on-chip free-flow magnetophoresis. *Lab Chip* **2006**, *6*, 974–980. [CrossRef] [PubMed]
18. Pamme, N. Continuous flow separations in microfluidic devices. *Lab Chip* **2007**, *7*, 1644–1659. [CrossRef] [PubMed]
19. Fraga-García, P.; Kubbutat, P.; Brammen, M.; Schwaminger, S.; Berensmeier, S. Bare Iron Oxide Nanoparticles for Magnetic Harvesting of Microalgae: From Interaction Behavior to Process Realization. *Nanomaterials* **2018**, *8*, 292. [CrossRef]
20. Ge, S.; Agbakpe, M.; Wu, Z.; Kuang, L.; Zhang, W.; Wang, X. Influences of surface coating, UV irradiation and magnetic field on the algae removal using magnetite nanoparticles. *Environ. Sci. Technol.* **2015**, *49*, 1190–1196. [CrossRef]

21. Toh, P.Y.; Ng, B.W.; Chong, C.H.; Ahmad, A.L.; Yang, J.-W.; Chieh Derek, C.J.; Lim, J. Magnetophoretic separation of microalgae: The role of nanoparticles and polymer binder in harvesting biofuel. *RSC Adv.* **2014**, *4*, 4114–4121. [CrossRef]

22. Barhoumi, L.; Dewez, D. Toxicity of superparamagnetic iron oxide nanoparticles on green alga Chlorella vulgaris. *BioMed. Res. Int.* **2013**, *2013*, 647974. [CrossRef] [PubMed]

23. Yadidia, R.; Abeliovich, A.; Belfort, G. Algae removal by high gradient magnetic filtration. *Environ. Sci. Technol.* **1977**, *11*, 913–916. [CrossRef]

24. Ge, S.; Agbakpe, M.; Zhang, W.; Kuang, L. Heteroaggregation between PEI-coated magnetic nanoparticles and algae: Effect of particle size on algal harvesting efficiency. *ACS Appl. Mater. Sci.* **2015**, *7*, 6102–6108. [CrossRef] [PubMed]

25. Turrina, C.; Berensmeier, S.; Schwaminger, S.P. Bare Iron Oxide Nanoparticles as Drug Delivery Carrier for the Short Cationic Peptide Lasioglossin. *Pharmaceuticals (Basel)* **2021**, *14*, 405. [CrossRef]

26. Cerff, M.; Morweiser, M.; Dillschneider, R.; Michel, A.; Menzel, K.; Posten, C. Harvesting fresh water and marine algae by magnetic separation: Screening of separation parameters and high gradient magnetic filtration. *Bioresour. Technol.* **2012**, *118*, 289–295. [CrossRef]

27. Li, Y.-G.; Gao, H.-S.; Li, W.-L.; Xing, J.-M.; Liu, H.-Z. In situ magnetic separation and immobilization of dibenzothiophene-desulfurizing bacteria. *Bioresour. Technol.* **2009**, *100*, 5092–5096. [CrossRef]

28. Schwaminger, S.P.; Bauer, D.; Fraga-García, P. Gold-iron oxide nanohybrids: Insights into colloidal stability and surface-enhanced Raman detection. *Nanoscale Adv.* **2021**, *3*, 6438–6445. [CrossRef]

29. Wittmann, L.; Turrina, C.; Schwaminger, S.P. The Effect of pH and Viscosity on Magnetophoretic Separation of Iron Oxide Nanoparticles. *Magnetochemistry* **2021**, *7*, 80. [CrossRef]

30. Kim, W.; Suh, C.-Y.; Cho, S.-W.; Roh, K.-M.; Kwon, H.; Song, K.; Shon, I.-J. A new method for the identification and quantification of magnetite-maghemite mixture using conventional X-ray diffraction technique. *Talanta* **2012**, *94*, 348–352. [CrossRef]

31. Schwaminger, S.P.; Schwarzenberger, K.; Gatzemeier, J.; Lei, Z.; Eckert, K. Magnetically Induced Aggregation of Iron Oxide Nanoparticles for Carrier Flotation Strategies. *ACS Appl. Mater. Interfaces* **2021**, *13*, 20830–20844. [CrossRef]

32. Santoyo Salazar, J.; Perez, L.; de Abril, O.; Truong Phuoc, L.; Ihiawakrim, D.; Vazquez, M.; Greneche, J.-M.; Begin-Colin, S.; Pourroy, G. Magnetic Iron Oxide Nanoparticles in 10−40 nm Range: Composition in Terms of Magnetite/Maghemite Ratio and Effect on the Magnetic Properties. *Chem. Mater.* **2011**, *23*, 1379–1386. [CrossRef]

33. Thomas, J.A.; Schnell, F.; Kaveh-Baghbaderani, Y.; Berensmeier, S.; Schwaminger, S.P. Immunomagnetic Separation of Microorganisms with Iron Oxide Nanoparticles. *Chemosensors* **2020**, *8*, 17. [CrossRef]

34. Tham, F.K.; Ng, W.M.; Leong, S.S.; Yeap, S.P.; Low, S.C.; Lee, H.L.; Lim, J. Magnetophoresis of Magnetic Pickering Emulsions Under Low Field Gradient: Macroscopic and Microscopic Motion. *Langmuir* **2021**, *37*, 1811–1822. [CrossRef] [PubMed]

35. Schwaminger, S.P.; Syhr, C.; Berensmeier, S. Controlled Synthesis of Magnetic Iron Oxide Nanoparticles: Magnetite or Maghemite? *Crystals* **2020**, *10*, 214. [CrossRef]

36. Baalousha, M. Aggregation and disaggregation of iron oxide nanoparticles: Influence of particle concentration, pH and natural organic matter. *Sci. Total Environ.* **2009**, *407*, 2093–2101. [CrossRef]

37. Baldassarre, F.; Cacciola, M.; Ciccarella, G. A predictive model of iron oxide nanoparticles flocculation tuning Z-potential in aqueous environment for biological application. *J. Nanopart. Res.* **2015**, *17*, 377. [CrossRef]

38. Bäumler, M.; Schwaminger, S.P.; von der Haar-Leistl, D.; Schaper, S.J.; Müller-Buschbaum, P.; Wagner, F.E.; Berensmeier, S. Characterization of an active ingredient made of nanoscale iron(oxyhydr)oxide for the treatment of hyperphosphatemia. *RSC Adv.* **2021**, *11*, 17669–17682. [CrossRef]

39. Mykhaylyk, O.; Lerche, D.; Vlaskou, D.; Schoemig, V.; Detloff, T.; Krause, D.; Wolff, M.; Joas, T.; Berensmeier, S.; Plank, C. Magnetophoretic Velocity Determined by Space- and Time-Resolved Extinction Profiles. *IEEE Magn. Lett.* **2015**, *6*, 1–4. [CrossRef]

40. Boulter, E.; Colombelli, J.; Henriques, R.; Féral, C.C. The LEGO®brick road to open science and biotechnology. *Trends Biotechnol.* **2022**, *40*, 1073–1087. [CrossRef]